Regular Article

Impact of Image Denoising Techniques on CNN-based Liver Vessel Segmentation using Synthesis Low-dose Contrast Enhanced CT Images

Le Quoc Anh[1], Pham Xuan Loc[2], Luu Manh Ha[1,2]

[1] AVITECH, University of Engineering and Technology, Vietnam National University, Hanoi, Vietnam
[2] FET, University of Engineering and Technology, Vietnam National University, Hanoi, Vietnam

Correspondence: Luu Manh Ha, halm@vnu.edu.vn
Communication: received 09 May 2022, revised 14 November 2022, accepted 15 December 2022
Online publication: 22 December 2022, Digital Object Identifier: 10.21553/rev-jec.315
The associate editor coordinating the review of this article and recommending it for publication was Prof. Vo Nguyen Quoc Bao.

Abstract– **Liver vessel segmentation in contrast-enhanced CT (CECT) images has a significant role in the planning stage for liver cancer treatment, such as radiofrequency ablation (RFA). Lowering the radiation dose in CECT imaging to reduce radiation risk to the patient degrades the quality of the image and potentially affects the liver vessel segmentation. In recent years, the convolutional neural network (CNN) has shown significant achievement in medical image analysis, including segmentation and denoising tasks. This paper presents a study on a new framework consisting of three well-known denoising techniques, including vessel enhancing diffusion (VED), RED-CNN, and MAP-NN, along with the state-of-the-art segmentation method (nnU-Net) to segment the liver vessels in CECT images. We quantitatively evaluate the impacts of denoising techniques on the vessel segmentation on multi-level simulated low-dose CECT images of the liver. The performances of the liver vessel segmentation method combined with the denoising techniques are evaluated using Dice score, sensitivity metric, and processing time. In addition, the effect of denoising on the surface roughness of the segmented liver vessel is also investigated. The experiments show that the image denoising techniques improve the quality of liver vessel segmentation on high noisy CECT images while also reducing the segmentation accuracy on low-noise-level CECT images.**

Keywords– **Liver vessel segmentation, CNN, low-dose CECT, RFA, MAP-NN, VED, RED-CNN.**

1 Introduction

Liver vascular analysis is an essential step in the diagnosis and treatment of liver-related diseases [1]. In the functional anatomy of the liver, information about the liver vascular system (especially the main branches) helps divide the liver lobes, assisting in performing several procedures such as resection and liver transplantation [2]. Liver vessel segmentation also allows rendering vascular information in 3D space, supporting the planning and implementation of interventional procedures in the liver area [3]. Radiofrequency Ablation (RFA) is a minimally invasive therapy used for liver cancer treatment and conventionally suitable for early-stage multi-tumor cases [4–6]. In clinical practice, the interventionist, under the guidance of US/CT image modality, inserts the ablator through the skin and right at the center of the tumor [7]. After an intensity current via the ablator is triggered, the tumor is destroyed by the local heat radiated from the tip of the ablator. RFA has several advantages, such as the low risk of death from treatment. In addition, patients who received treatment with RFA can return home on the same day and recover in only a few days [5].

The limitation of RFA is a high local recurrence rate for tumors larger than 3 cm and abutting large vessels [8]. Since the early years of the 21st century, studies on the influence of blood vessels on RFA therapy have been investigated [9, 10]. It has been reported that the rate of treatment failure is more significant than 40% in cases with tumors abutting large vessels [11]. Indeed, the major limitation of RFA is that the heat is affected by the liver parenchyma and large vessels abutted tumors, which is called the heat-sink effect [11]. Lu *et al*. [9] determined that the appearance of blood vessels from 3 mm in diameter affects the failure to destroy the tumor when intervening with RFA. Huang [12] simulated the RFA heat treatment and suggested the RF cool-tip electrode placement treat lesions abutting large vessels. Loriaud *et al*. [11] investigated the comparison among percutaneous ablation systems in the treatment of liver tumors connecting large vessels ($>$ 3 mm in diameter). Therefore, analyzing the larger liver vessels near the tumor is essential in the planning stage of RFA liver cancer intervention.

CECT images are commonly used in the RFA procedure, which provides information about liver anatomy without invasive procedures [7, 13]. However, the radiation dose of the CT images involves a particular risk for the patient, such as radiation-induced cancer [14, 15]. Consequently, lowering the radiation dose is preferably performed on the CECT image to reduce the risk for the patient, which increases the low-dose noise in the

CECT images. The low-dose noise affected the subtle details in the CT image, including small vessels, leading to a challenge of liver vessel segmentation. In previous studies, vessels were manually identified by radiologists in 2D slices [9]. This manual work is often user dependent and has low reproducibility. Therefore, (semi)automatic liver vessel segmentation based on the computer-assisted approach has been highly active in the research field. Nevertheless, liver vessel segmentation is still challenging due to the varying and complicated vessel structure [3]. Image-related challenges also increase the difficulty of liver vessel segmentation, including diverse contrast between the vessel and surrounding tissues and images with a low-quality [16].

The rapid development of deep learning in medical image analysis has recently created many practical techniques for the segmentation task. However, research on applying deep learning techniques to segment the liver vessels in CECT images for the planning phase of the ablation treatment is still limited. Through the literature review, we found that although several liver vessel segmentation methods have already been developed, liver vessel segmentation for low-dose CECT images needs to be investigated more thoroughly. Therefore, this study aims to investigate the impact of low-dose noise on the liver vessel segmentation performance; and then further investigate the impact of the denoising technique on the improvement of the liver vessel segmentation with attention to the large liver vascular area. This study is a further development of our previous work published in conferences where we have already compared several CNN-based liver vessel segmentation methods and several denoising methods [13, 17]. To achieve the aim above, we first simulate multiple levels of low-dose noise on normal-dose CT images. Subsequently, we investigate the impact of several state-of-the-art denoising techniques on liver vessel segmentation performance by a CNN-based method which was verified in our previous study [17]. Finally, we assess the roughness of the surface of the large vessel segmentation under the impact of the denoising techniques.

2 Related Works

2.1 Vessel Segmentation Method

Several liver vessel segmentation methods have been proposed in the literature and are potentially applicable to clinical applications. In general, those methods can fall into two main groups [3, 16]. The group of classical image processing methods mainly uses filters to reduce noise and enhance the contrast of the vessel with surrounding liver tissue, and then apply morphological techniques to predict the liver vessel segmentation [13, 18]. However, the classical methods have limitations. They require the user to carefully identify the dataset's properties and select suitable parameters for segmentation. With the vigorous development of computer hardware in the past decade and many published open-source datasets, the group of methods for applying deep learning techniques has shown its effectiveness in medical image analysis [19, 20]. Huang *et al*. [3] introduced 3D-UNet combination with a variant of the Dice loss function and studied the effect of data labeling on the accuracy of the liver vessel segmentation. Yu *et al*. [21] combined ResNet architecture with 3D UNet to create 3D ResUNet architecture for liver vessel segmentation. Kitrungrotsakul *et al*. [19] proposed a liver vessel segmentation method that uses three convolutional neural networks for feature extraction from three different planes of CT scans. Su *et al*. [20] also proposed a DV-Net architecture for vessel segmentation. Isensee *et al*. [22] published a robust framework for the task of image segmentation. nnU-Net uses UNet architecture combined with an automatic parameters configuration method, enabling high accuracy in many image segmentation tasks.

2.2 Low-dose Denoising Method

Recently, denoising low-dose noise in CT images has been dramatically interested to the research community. Many low-dose noise reduction methods have been published in the literature. Generally, the denoising methods can be divided into two groups. The first group removes the low-dose noise from the projection image [23, 24], and the second group eliminates the noise from the CT image [25–27]. In the first group, filters are used to filter the projection images and then reconstruct CT images using interactive techniques or filter back-projection methods. However, the raw projection image source is not often available since it is embedded in the CT scan machine. Then, many researchers attend to denoising the low-dose noise on the CT image. Most classical methods defined the low-dose noise on CT images as approximated Gaussian distribution [28]. However, the low-dose noise in the CT image is not easy to be precisely estimated, which may affect the performance of the classical method. Manniesing *et al*. [25] introduced the vessel enhancing diffusion that used sparse representation to improve the visualization of the vessels in low-dose CT scans. Recently, The CNN has been investigated in the low-dose CT scan denoising with the development of deep learning techniques. Chen *et al*. [26] proposed the RED-CNN, which is the first study on applying the deep learning technique for low-dose denoising in CT images. Shan *et al*. [27] compare the performance of deep learning techniques with a commercial algorithm for reducing the low-dose noise in CT images. The results show that deep learning has comparable performance on low-dose noise reduction with the iterative reconstruction algorithm.

3 Methods

This section briefly describes the techniques we use in our framework for simulating the low-dose noise in CECT images, denoising, and segmenting the liver vessels.

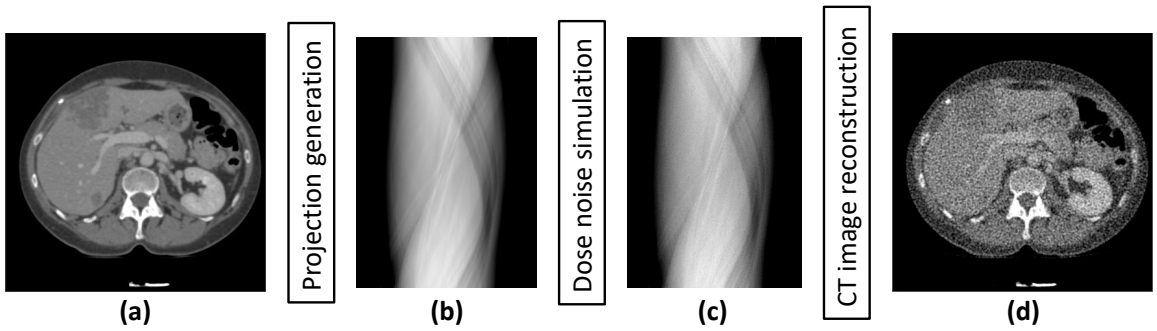

Figure 1. The process of the low-dose noise simulation. (a) the normal-dose CECT image, (b) the simulated projection image from the normal-dose CECT image, (c) the projection with the Poisson noise, (d) the simulated low-dose CECT image.

3.1 Low-dose Simulation Technique

To obtain multiple levels of low-dose noise on CECT images, we simulate the number of photon counts on normal-dose CECT images with the contrast-to-noise (CNR) of the vessel area higher than 6.0 (see Section 4.4). The low-dose noise simulation technique is reused from the research of Leuschner *et al.* [29]; the process of low-dose noise simulation is presented in Figure 1. First, we utilized all CECT image sizes of 512×512 to create the projection image using Radon transform:

$$\mathcal{A}x(s,\varphi) := \int_{\mathbb{R}} x\left(s\begin{bmatrix}\cos(\varphi)\\ \sin(\varphi)\end{bmatrix} + t\begin{bmatrix}-\sin(\varphi)\\ \cos(\varphi)\end{bmatrix}\right) dt, \tag{1}$$

where $\mathcal{A}$ is the linear ray transform, x denotes the projection of attenuation coefficient along the ray path s, where s is the distance from the origin, and φ is the angle of the beam in the parallel beam CT model.

Subsequently, the projection images were added with Poisson noise to simulate the low-dose noise level. The number detector photon $\tilde{N}_1$ can be modeled as the follows:

$$\tilde{N}_1(s,\varphi) \sim \text{Pois}\left(N_0 \exp(-\mathcal{A}x(s,\varphi))\right), \tag{2}$$

where $\text{Pois}(\lambda)$ is Poisson distributed; N_0 represents the mean number photon count; when changing the value of N_0, we obtain the corresponding low-dose noise level in the simulated noisy CT image. Finally, a filtered back-projection reconstructs the dose noise simulation CECT images using Hann filter.

3.2 Denoising Techniques

3.2.1 Vessel Enhancing Diffusion: VED, introduced by Manniesing *et al.* [25], is a Hessian-based diffusion filter that was designed to enhance the vessel-like structure in noisy images. It uses eigenvalues of the Hessian matrix to establish a diffusion tensor D_V to measure curvature at the voxel level. The key idea of VED is that it diffuses to smooth only along the vessel while preserving the vessel wall. The vesselness function is $V \in [0,1]$ as the output of the multiscale scale vesselness filter so that V reaches 1 at the voxels inside vessel-like structures and 0 elsewhere. If $|\lambda_1|$, $|\lambda_2|$ and $|\lambda_3|$ are the eigenvalues of Hessian matrix H, such that $|\lambda_1| < |\lambda_2| < |\lambda_3|$, corresponding to the eigenvectors Q_1, Q_2 and Q_3 which satisfy $H = Q.\Lambda.Q^T$; we then have Q_1 as the direction of the slightest curvature. Subsequently, we can define the diffusion tensor as $D_V = Q.\Lambda'.Q^T$, in which the diagonal elements of matrix Λ' are defined as:

$$\begin{cases}\lambda_1' = 1 + (\omega - 1)V^{1/S},\\ \lambda_2' = \lambda_3' = 1 + (\varepsilon - 1)V^{1/S},\end{cases} \tag{3}$$

where ω is a parameter larger than 1 to guarantee that Q_1 is the largest diffusion direction; ε is a minimal value that enables high isotropic diffusion when $V \approx 0$ (at non-vessel structure); and S is a predefined parameter which moderates the impact of V on λ_1'.

3.2.2 The residual encoder-decoder convolutional neural network: RED-CNN is one of the first techniques to apply CNN to solve the problem of low-dose noise reduction in CT images [26], also known as an inverse problem. The basic idea of RED-CNN is to use a CNN to use supervised learning to estimate the property of the noise from low-dose CT images, given the corresponding normal-dose CT images. RED-CNN contains three main parts: autoencoder, deconvolution network, and shortcut connections. The end-to-end network is similar to the architecture of the UNet network in the segmentation problem [30]. Unlike UNet, RED-CNN only uses convolution blocks and ReLU units instead of pooling layers to guarantee the essential structural details. The training of the RED-CNN model is to optimize a set of convolution and deconvolution layer parameters Θ to construct a mapping function M for low-dose noise reduction. Specifically, it minimizes the difference between the estimated CT images from the noisy CT images via the current state of the on-training model and the reference normal-dose CT images, called loss function $F(\Theta)$. Mathematically, given a set of N pair images used for training $P = \{(\boldsymbol{X}_1, \boldsymbol{Y}_1), (\boldsymbol{X}_2, \boldsymbol{Y}_2), \ldots, (\boldsymbol{X}_N, \boldsymbol{Y}_N)\}$ where $\boldsymbol{X}$ and $\boldsymbol{Y}$ represents for normal-dose CT image and low-dose CT image, the loss function of RED-CNN is defined as follows:

$$F(\Theta) = \frac{1}{N}\sum_{i=1}^{N} \|\boldsymbol{X}_i - M(\boldsymbol{Y}_i)\|^2. \tag{4}$$

3.2.3 The modularized adaptive processing neural network: MAP-NN was introduced by Shan *et al.* for low-dose denoising in CT images [31]. Similar to RED-CNN,

Table I
The Properties of the Dataset for Training and Dose Simulation

Dataset		Number of CT images	Number of slices	In plane resolution (mm)	Spacing between slices (mm)
Pre-trained	**MSD**	303	24 - 181	0.57 - 0.98	0.8 - 8.0
Training	**IRCADB**	12	76 - 249	0.56 - 0.81	1.0 - 2.0
	EMC	18	44 - 99	0.60 - 0.86	2.0 -3.0
	SLiver07	8	49 - 217	0.59 - 0.74	1.0 - 5.0
Low-dose simulation	**IRCADB**	3	51 - 106	0.57 - 0.74	1.6 - 4.0
	EMC	6	55 - 64	0.64 - 0.68	3.0
	SLiver07	6	36 - 185	0.57 - 0.75	1.0 - 3.0

MAP-NN uses CNN to solve the inverse problem. The architecture of MAP-NN is composed of multiple CPCE blocks concatenated together and uses skip connections to retrieve information from the previous block, called the functional composition operation ($\circ$). The denoised image ($\hat{\boldsymbol{Y}}$) of MAP-NN is defined as follows:

$$\hat{\boldsymbol{Y}} = g^T(\boldsymbol{Y}) = \underbrace{(g \circ g \circ \cdots \circ)g}_{T=\#g}(\boldsymbol{Y}), \tag{5}$$

where g denotes a CPCE block. The Wasserstein generative adversarial (WGAN) is used to improve stability when training the MAP-NN model. The WGAN includes two networks (G, D), where G is utilized for denoised image generation that most resembles the reference image, while D is used to distinguish between the denoised and reference image. To update the parameters of G, MAP-NN uses three loss functions, including Adversarial loss ($\mathcal{L}_a$), MSE loss ($\mathcal{L}_m$), and Edge incoherence loss ($\mathcal{L}_e$). The final object function for optimizing the G parameters (θ_g) of MAP-NN is defined as follows:

$$\min_{\theta_g} \mathcal{L} = \mathcal{L}_{\mathrm{a}} + \lambda_{\mathrm{m}}\mathcal{L}_{\mathrm{m}} + \lambda_{\mathrm{e}}\mathcal{L}_{\mathrm{e}}, \tag{6}$$

where λ_{m} and λ_{e} denote the weight to balance the loss terms.

3.3 Liver Vessel Segmentation

In this study, we use nnU-Net, published by Isensee *et al*. [22], as the reference method for liver vessel segmentation in CECT images as it obtained a high ranking in a public liver vessel segmentation challenge [32], and also was verified in our previous study [17]. nnU-Net is an open-source CNN-based framework for segmentation in medical images. Inheriting the success of UNet in the medical image segmentation field, nnU-Net has a similar architecture to UNet, which contains two parts: encoder and decoder. nnU-Net haves some minor changes, including using the activation function Leaky ReLU instead of ReLU and using instance normalization instead of batch normalization. The distinguished property of nnU-Net is that the preprocessing stage can automatically be configured depending on the training dataset. nnU-Net allows using two types of networks based on 2D or 3D input for convenient and accurate segmentation. In this study, to take advantage of inter-slice information, we use 3D nnU-Net model to conduct the segmentation. Before using nnU-Net for segmentating the liver vessel, its model should be trained for specify data. In this study we resused the pre-train model trained with a public datasets and fine-turned with both public and private datasets. The experimental details are described in the experiment section (section 4).

4 Experiment

4.1 Dataset

The data used in this study was collected from multiple medical centers and cataloged into three subsets with a total of 50 CT images containing 4327 2D CT slices for training and 15 CT images with 1456 2D CT slices for evaluating the dose simulation technique, the denoising techniques, and the liver vessel segmentation technique. The properties of the dataset are listed in Table I.

The first dataset is an open-source 3Dircadb-01 (IRCADB) widely used in studies on liver vessel segmentation. We choose 12 CT scans for training the vessel segmentation model and 3 CT scans for the simulation phase. The second dataset was collected from the liver segmentation challenge organized by MICCAI in 2007 (Sliver07), which was suggested for use by studies on liver vessel segmentation; we selected 8 CT scans for training and 6 CT scans for the simulation phase.

The remaining dataset was collected from Erasmus Medical Center (EMC). The datasets were approved for research by the local ethic committee. We used 30 CECT scans and 6 CECT scans collected during the diagnosis and treatment of liver cancer using the RFA technique at EMC for the training and simulation stages, respectively.

The chosen images for the simulation stage have low noise with contrast-to-noise (CNR) of the vessel areas higher than 6.0, which are qualitatively determined using the CNR criteria described in the experiment section 4.4. The ground truth for liver vessel segmentation is manually annotated by an experienced technician and then verified by an expert.

Recently, Medical Segmentation Decathlon (MSD) challenge has published a large amount of data, including 303 CT scans for liver vessel segmentation purposes with annotated liver vessel [32]. To take advantage of the CNN-based approach, we reuse the

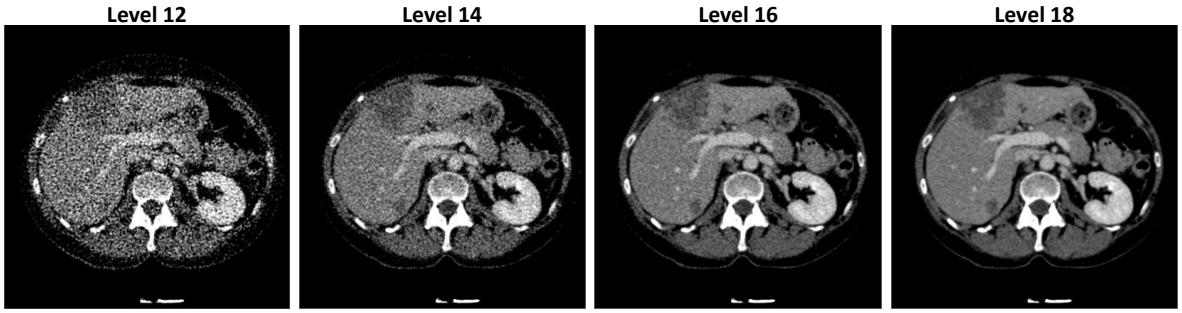

Figure 2. An example of dose level simulation on a normal-dose CECT images. The lower levels indicate more low-dose noise inducted in the images.

nnU-Net model trained on MSD dataset [22] as the pre-trained model and fine-tune the model using the training dataset in this study.

4.2 Preprocessing

We limit the prediction area by using the liver mask before putting the CT images into the model nnU-Net to predict the liver vessel segmentation. The generated liver mask was investigated in our previous study [17], which is the predicted liver segmentation passes through the morphology operator with kernel size (X, Y, Z) of (30, 30, 1). In addition, we exclude the IVC region in this study since it is a large vessel and could alter the evaluation of liver vessel segmentation performance.

4.3 Implementation and Training

We deploy the vessel segmentation method, nnU-Net, on Python 3.8 using Pytorch 1.7 on top of CUDA 11.2. The nnU-Net was initialized from the pre-trained model and fine-tuned with 500 epochs; the initial learning rate was set at 10^{-2}, and decayed as in the default setting. We use stochastic gradient descent optimizer with Nesterov momentum of 0.99 for the training with the total fine-tuning time around 12 hours.

For denoising techniques, we implement the VED with ITK version 4.10 with the parameters suggested by Luu *et al*. [13]. The implementation and the parameters of RED-CNN and MAP-NN are provided by the authors [26, 31].

We identify the large liver vessels in section 4.6.1 uses the library VMTK[1] integrated into the 3D Slicer software package.

This study was carried out on an Ubuntu 20.04 operating system computer with an Intel® Core™ i9 10900 processor, 64 GB DDR4. The training was performed using an NVIDIA RTX 8000 (48 GB VRAM) and the vessel segmentation was obtained using an NVIDIA RTX 3090 GPU (24 GB VRAM).

4.4 Experiment 1: The image quality analysis on simulated low-dose CT images

4.4.1 Experiment setup: The goal of this experiment is to verify the dose simulation technique mentioned in section 3.1 via assessing the noise level. In the research of Leuschner *et al*. [29], the mean photon count N_0 was set at 4096 (i.e. 2^{12}) for ultra-low-dose simulation. However, in clinical practice, the CT images with the ultra-low-dose level are rare, so we define that as the lowest dose simulation level (level 12). Next, we increase the value of N_0 to simulate the other eight low-dose levels with the mean photon counts from 2^{13} to 2^{20}, corresponding to the low-dose simulation level of 13 to 20, respectively. Subsequently, for each simulation level, the generated noise is added to the projection image before projecting back to the image space using the invert Radon transform (see section 3.1). Figure 2 illustrates an example image with several generated noise levels.

4.4.2 Evaluation criteria: To assess the image quality under the effect of low-dose simulation, we use contrast-to-noise (CNR) metric that were suggested by some of the researches on the quantitative quality of low-dose CT images [13, 33]

$$CNR = \frac{m_v - m_l}{\sqrt{\frac{1}{2} \times (sd_{ve}^2 + sd_{lp}^2)}}, \tag{7}$$

where m_{ve} and m_{lp} are the mean intensity of the vessel and liver parenchyma region, respectively. sd_{ve} and sd_{lp} are the standard deviation of of the vessel and liver parenchyma region, respectively.

4.5 Experiment 2: Segmentation score of the three denoising techniques on simulated low-dose CT images

4.5.1 Experiment setup: This section presents an experiment to verify the effect of dose simulation and denoising the liver vessel segmentation. Firstly, this study performs dose noise simulation using normal-dose CT images, with nine noise levels based on the mean photon count presented in experiment 4.4. Subsequently, we perform the three denoising techniques (VED, RED-CNN and MAP-NN) to denoise the simulated low-dose CECT images. Finally, the liver vessels on the denoised CT images are extracted using nnU-Net.

4.5.2 Evaluation criteria: To evaluate the impact of denoising techniques for the vessel segmentation, two standard metrics in studies of vessel segmentation were used [3, 20] including sensitivity (SEN) and Dice similarity coefficient (DSC).

[1] http://www.vmtk.org/

Dice score:

$$DSC = \frac{2 \times TP}{(TP + FP) + (TP + FN)}, \tag{8}$$

Sensitivity:

$$SEN = \frac{TP}{TP + FN}, \tag{9}$$

where TP, FP, and FN are the number of true positive, false positive, and false negative of pixels, respectively.

4.6 Experiment 3: Surface roughness synthesis

4.6.1 Experiment setup: In this experiment, we evaluate the effect of the denoising methods on the roughness surface of large vessel segmentation from the dose simulation CT images. We utilize the vessel segmentation from the experiment 4.5 and limited the vessel range using the large vessel mask extracted from the ground truth. The process of large vessel extraction is reused from our previous study [17]. First, the vessel's centerline is extracted using the start point and the endpoint of the vessel branch. The vessel radius is calculated by using an inscribed sphere. Subsequently, for vessel branches which have a radius smaller than 3 mm, we create a sphere at the start point of this branch and remove all pixels inside this sphere. Finally, the large vessels are retrieved after keeping the largest connected component.

4.6.2 Evaluation criteria: Surface roughness

The surface roughness is computed by using the roughness estimation method introduced by Lavoue [34]. This method is efficient for estimating local roughness, which is helpful for quality metrics. There are four steps to estimate the roughness value of each vertex in a mesh: (1) The original mesh is smoothed using the adaptive smoothing filter based on the Taubin filter; (2) The curvature value ($kmax$) of each vertex in two mesh (original and smoothed) is calculated using the Normal Cycle; (3) Each vertex's average value (kav) is estimated using the local window analysis; (4) The roughness value of vertex v is estimated as follows:

$$R(v) = \begin{cases} kav(v) - kav\left(v^s\right) & \text{if } kav(v) > kav\left(v^s\right), \\ 0 & \text{else,} \end{cases} \tag{10}$$

where v and v^s correspond to the original and smoothed mesh vertex; the average roughness metric (R_a) is used to compare the roughness of different meshes and calculated as the mean of the roughness value of all the vertexes in its mesh.

5 Results

5.1 Result of experiment 1: The image quality analysis on simulated low-dose CT images

Figure 3 presents the average CNR value of the synthesis low-dose CECT images w.r.t dose simulation level. It can be seen that for the original images, the average CNR is higher than 6.0. Once the simulation level decrease, i.e., the number of simulated photon counts decreases, more noise is inducted into the image,

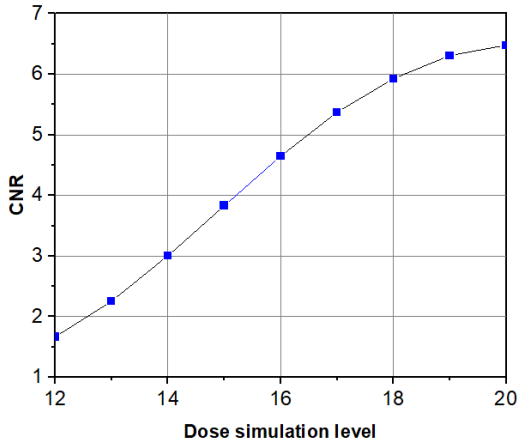

Figure 3. Average CNR score of liver vessel region on the simulated dataset w.r.t dose level simulation.

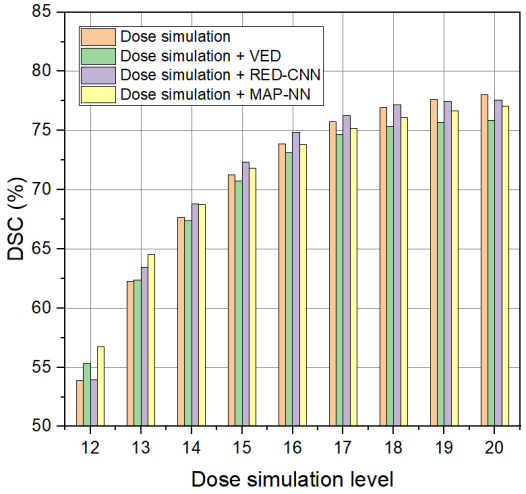

Figure 4. Average DSC score of the liver vessel segmentation on the simulated dataset w.r.t dose level simulation.

and the average CNR reduces to 1.67. According to Hamard *et al*. [33], a normal-dose CECT image has a CNR greater than 6.0 (or 7.78 dB). For ultra-low-dose images with a CNR less than 4.0, our simulated noise levels are 12 to 15 (CNR from 1.67 to 3.83), corresponding to the ultra-low-dose level. The simulated noise levels from 16 to 18 (CNR from 4.65 to 5.93) correspond to moderate low-dose noise.

5.2 Result of experiment 2: Segmentation score of three denoising techniques on synthesis low-dose CT images

This experiment evaluates two segmentation metrics, including DSC score and sensitivity, to assess the impact of three denoising techniques on segmenting the liver vessel. Figure 4 indicates that the vessel segmentation accuracy is proportional to the simulated low-dose level. Evaluating the liver vessel segmentation on the simulated low-dose CT images, the DSC score reaches 53.9% at the lowest simulated level and increases gradually at the following levels. Additionally, applied denoising techniques improve the vessel segmentation accuracy at the simulated level smaller than 18. MAP-NN achieves better accuracy at levels 12 and 13 than the

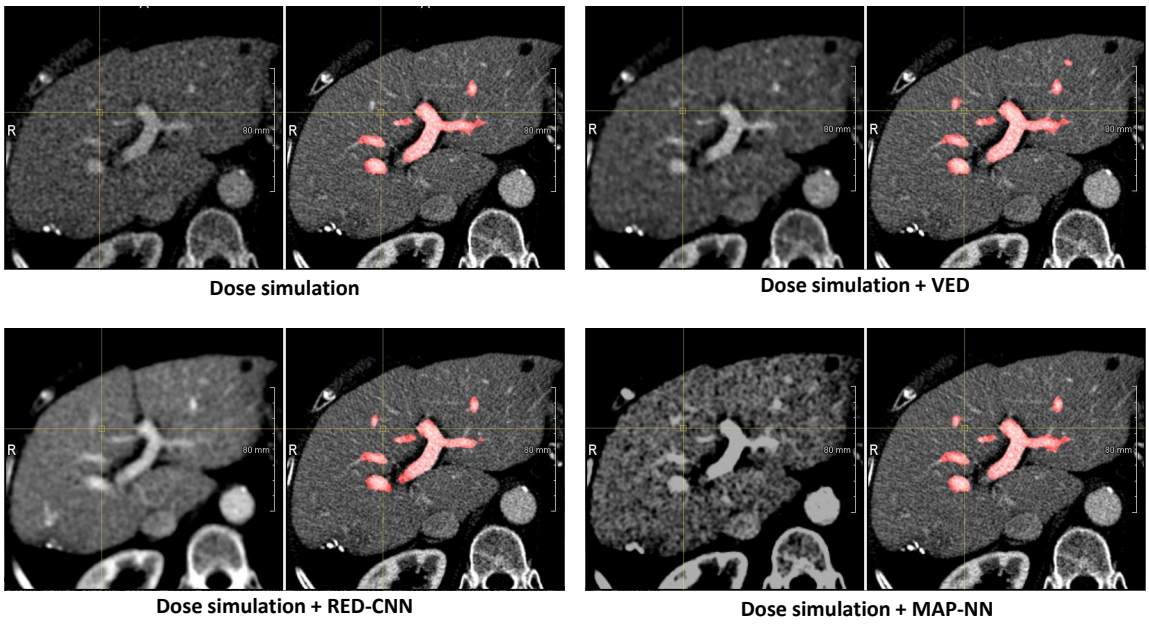

Figure 5. An example of liver vessel segmentation on synthesis low-dose noise CECT slice at simulation level 14, with and without denoising techniques.

Table II
Average Sensitivity of Vessel Segmentation on Simulated Dataset w.r.t Simulated Dose Level. The Higher Simulation Level Means the Lower Noise Affection on the Images

Simulation level	12	13	14	15	16	17	18	19	20
Dose simulation	41.5%	52.3%	61.2%	67.5%	72.9%	76.5%	78.8%	**80.5%**	**81.4%**
Dose simulation + VED	**45.6%**	54.5%	61.5%	66.8%	71.4%	74.4%	76.4%	77.5%	78.0%
Dose simulation + RED-CNN	41.5%	53.8%	62.5%	**68.5%**	**73.5%**	**76.7%**	**78.8%**	80.3%	80.9%
Dose simulation + MAP-NN	44.8%	**56.0%**	**63.2%**	68.2%	72.1%	74.2%	76.0%	77.3%	78.1%

Table III
Average Processing Time of the Denoising and Vessel Segmentation Process. The Unit is in Seconds

Processing time	Low-dose denoising	Vessel segmentation
Dose simulation	-	19.8
Dose simulation + VED	775.7	20.5
Dose simulation + RED-CNN	30.6	19.7
Dose simulation + MAP-NN	18.2	20

remainder denoising methods. Meanwhile, RED-CNN shows more effectiveness in liver vessel segmentation at levels 15 to 18. However, vessel segmentation accuracy is reduced when the denoising methods are applied at low-noise levels (i.e., levels 19 and 20).

Table III shows the sensitivity of liver vessel segmentation that represents the ability to detect the liver vessels in CT images. Figure 5 shows an example of liver vessel segmentation on a noisy CECT image with and without using the denoising techniques. It can be seen that without applying the denoising technique, the segmentation method ignores some of the vessel regions that are affected by the low-dose noise.

Table II displays the average processing time of the denoising techniques. It can be seen that VED is a classic method and only uses a CPU, which makes the average computation time up to 775.7 seconds to perform a CT scan. Meanwhile, RED-CNN and MAP-NN have taken advantage of modern computer hardware (GPU) and get an average processing time of 30.6 and 18.2 seconds. Additionally, the denoising techniques do not affect the processing time of nnU-Net, which takes about 20 seconds on average for segmenting the vessel.

5.3 Result of experiment 3: Surface roughness

From Table IV, VED shows better liver vessel segmentation results on the lowest dose simulation level, which achieved the SEN value and the roughness surface of 45.6% and 0.341, respectively. However, the performance of the CNN-based techniques on denoising shows potential with the higher dose simulation level, which achieved better results than the VED. From Figure 6, it can be seen that if denoising is not applied, the liver vessel segmentation method ignores some vessel branches. Meanwhile, with the denoising methods applied, some vascular areas are retained. However, some vessel branches are still mislabeled due to the significant low-dose effect.

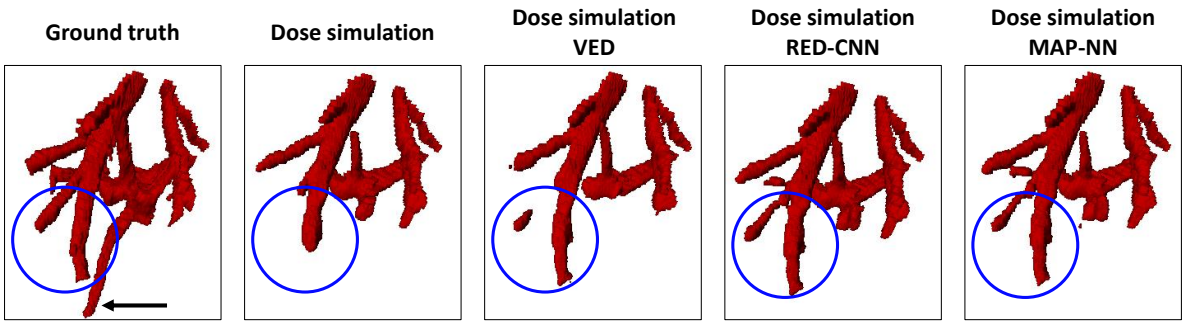

Figure 6. An example of liver vessel segmentation after excluding small vessel branches on synthesis CECT image at the simulation level 13. The blue circle shows some mislabeling on the vessel segmentation. The black arrow shows that all denoising methods mislabeled a vessel branch due to the significant noise.

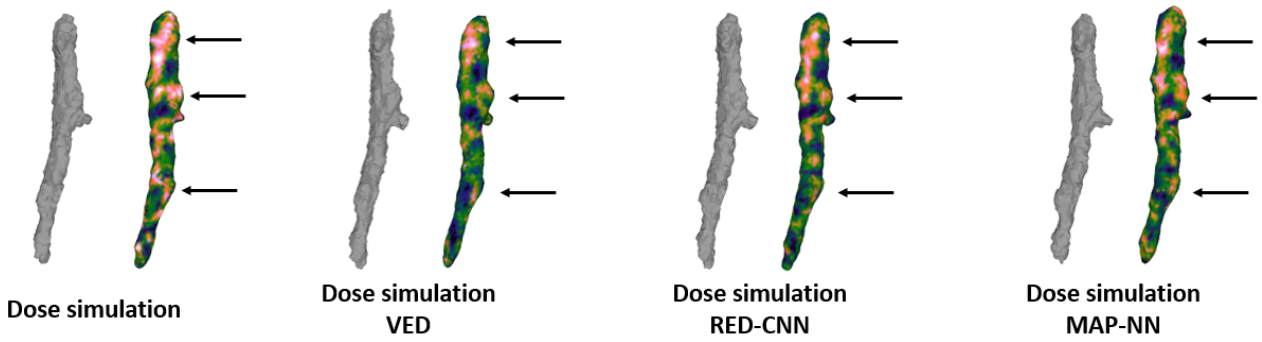

Figure 7. An example of roughness estimation on a large liver vessel branch at simulation level 12: The gray images represent the mesh surface generated from the binary vessel segmentation. The color images illustrate the roughness map of the corresponding meshing. The hot colors indicate high roughness surface, while the cool colors account for a low roughness surface.

Table IV
Average Surface Roughness of the Large Vessel Segmentation

Simulation level	12	13	14	15	16	17	18	19	20
Dose simulation	0.358	0.324	0.288	0.265	0.251	0.257	0.236	0.242	**0.239**
Dose simulation + VED	**0.341**	0.292	0.294	0.282	0.260	**0.247**	0.259	0.261	0.252
Dose simulation + RED-CNN	0.348	0.300	**0.270**	0.261	**0.238**	0.249	0.237	**0.239**	0.247
Dose simulation + MAP-NN	0.345	**0.274**	0.287	**0.258**	0.267	0.251	**0.233**	0.241	0.250

6 Discussion

In the first experiment, we simulated multiple levels of low-dose noise on normal-dose CECT images and assessed the simulated image quality using the CNR criteria. The CNR presents a ratio of the difference in intensity value between two regions in the image over the value of noises in the vessel and the background areas. It relates to the ability to distinguish the liver vessel region from the liver parenchyma area. Through the experiment, the CNR value decreased when reducing the simulated mean photon count. This result is consistent with the result reported in the study of Hamard *et al.* [33].

The second experiment investigated the effect of low-dose noise on vessel segmentation. It can be seen that under the heavily low-dose noise affection, the vessel segmentation method achieves poor results. Comparing the accuracy of liver vessel segmentation between the synthesis of low-dose noise CECT images at the highest and lowest level, the DSC score and sensitivity value significantly reduce from 78% to 53.9% and 81.4% to 41.5%, respectively. It can be explained that the effect of the low-dose noise might blur subtle details. As a result, the liver vessel segmentation method can not distinguish between the noise effect and the subtle details. This phenomenon was also pointed out in the study of Manniesing *et al.* [25].

The experiment results also showed that denoising methods degrade vessel segmentation accuracy when there is almost no low-dose noise (levels 19 and 20). We can see from Figure 5 that the use of the VED method decreases the variation of noise without much affecting the large vessel wall. However, the diffusion operator also blurs small vascular areas, causing a reduction in vessel segmentation accuracy at low-noise levels. Besides, the denoising method using deep learning is trained on Mayo dataset with low-dose noise at quarter-dose [35]. When applying the denoising techniques to normal-dose imaging, vessel segmentation accuracy is reduced. At the simulation level 15, with the denoising technique using RED-CNN, the vessel segmentation on the synthesis of low-dose noise CECT images achieved a DSC of 72.8%, yielding a comparable performance to

most of the top-rank liver vessel segmentation methods in MSD challenge [32]. Moreover, from Figure 4 and Table III, we can indicate that the CNN-based denoising techniques seem to perform a bit better than the VED denoising technique at the moderate simulation levels.

Anatomically, the vessel wall is smooth, and thus modeling the surface of blood vessels from CECT images is essential in liver vascular analysis. In the third experiment, we evaluated the surface roughness of the liver vessels on CECT images with multiple low-dose noise levels. The influence of low-dose noise can be seen on the surface roughness value (see Figure 7). We hypothesize that the smaller surface roughness is, the more closely similar the liver vessel can be modeled to the actual liver vessel information is. By applying the denoising methods, the surface roughness value has been reduced compared to the highly simulated image, indicating the potential to use the denoising method for low-dose noise reduction on CT images.

This study still has some limitations. First, the denoising methods used in this study were optimized with the parameters for a single level of noise provided in Mayo dataset. The analysis of parameters optimization for each low-dose level may need to be studied more in detail. Further more, training the denoising model for each noise level may improve the efficiency of liver vessel visualization and segmentation. In addition, we only use 15 simulation images to investigate the effect of low-dose noise on the liver vessel segmentation. We expect the further study may include more data in the evaluation stage to make the findings in this study more solid.

7 Conclusion

In summary, this paper has addressed the impact of denoising techniques on low-dose CT images for the task of liver vessel segmentation using CNN. We simulated multiple noise levels from 15 normal-dose CECT images of the liver and then used denoising techniques to suppress the low-dose noise independently. Subsequently, liver vessel segmentations were extracted using nnU-Net model, which was pre-trained using a public dataset and then fine-tuned using both public and private datasets. Based on the results from the experiments of liver segmentation and surface roughness evaluation, we conclude that for the low-noise CECT images, direct segmentation without denoising should be preferred. In contrast, when the images contain a large amount of low-dose noise, the CNN-based denoising methods should be applied to improve the quality of liver vessel segmentation.

Acknowledgment

This research is funded by Vietnam National Foundation for Science and Technology Development (NAFOSTED) under grant number 102.01-2018.316. We would like to thank Mayo Clinic for sharing the CT images. We would like to thank Prof. Theo van Walsum from Erasmus MC for the suggestion in this study. We also would like to thank Assoc. Prof. Dr. Dao Hang from Hanoi Medical University Hospital for the valuable discussion about the anatomy of liver vessel. We would like to thank Dr. Le Vu Ha for helping us in this research. We also would like to thank NVIDIA cooperation for supporting the graphic card RTX 8000 for this study.

References

[1] D. Selle, B. Preim, A. Schenk, and H.-O. Peitgen, "Analysis of vasculature for liver surgical planning," *IEEE Transactions on Medical Imaging*, vol. 21, no. 11, pp. 1344–1357, 2002.

[2] A. Nazir, M. N. Cheema, B. Sheng, P. Li, J. Kim, and T.-Y. Lee, "Living donor-recipient pair matching for liver transplant via ternary tree representation with cascade incremental learning," *IEEE Transactions on Biomedical Engineering*, 2021.

[3] Q. Huang, J. Sun, H. Ding, X. Wang, and G. Wang, "Robust liver vessel extraction using 3D U-Net with variant dice loss function," *Computers in Biology and Medicine*, vol. 101, pp. 153–162, 2018.

[4] H. Rhim and H. K. Lim, "Radiofrequency ablation of hepatocellular carcinoma: pros and cons," *Gut and liver*, vol. 4, no. Suppl 1, p. S113, 2010.

[5] I. Gory, M. Fink, S. Bell, P. Gow, A. Nicoll, V. Knight, A. Dev, A. Rode, M. Bailey, W. Cheung, *et al.*, "Radiofrequency ablation versus resection for the treatment of early stage hepatocellular carcinoma: a multicenter australian study," *Scandinavian Journal of Gastroenterology*, vol. 50, no. 5, pp. 567–576, 2015.

[6] F. Poch, C. Neizert, B. Geyer, O. Gemeinhardt, L. Bruder, S. Niehues, J. Vahldiek, K. Bressem, M. Kreis, and K. Lehmann, "Influence of interapplicator distance on multibipolar radiofrequency ablation during physiological and interrupted liver perfusion in an in vivo porcine model," *Scientific Reports*, vol. 10, no. 1, pp. 1–8, 2020.

[7] H. M. Luu, C. Klink, W. Niessen, A. Moelker, and T. v. Walsum, "Non-rigid registration of liver ct images for ct-guided ablation of liver tumors," *PloS one*, vol. 11, no. 9, p. e0161600, 2016.

[8] P. J. Littrup, H. D. Aoun, B. Adam, M. Krycia, M. Prus, and A. Shields, "Percutaneous cryoablation of hepatic tumors: long-term experience of a large US series," *Abdominal Radiology*, vol. 41, no. 4, pp. 767–780, 2016.

[9] D. S. Lu, S. S. Raman, P. Limanond, D. Aziz, J. Economou, R. Busuttil, and J. Sayre, "Influence of large peritumoral vessels on outcome of radiofrequency ablation of liver tumors," *Journal of Vascular and Interventional Radiology*, vol. 14, no. 10, pp. 1267–1274, 2003.

[10] C. Welp, S. Siebers, H. Ermert, and J. Werner, "Investigation of the influence of blood flow rate on large vessel cooling in hepatic radiofrequency ablation/untersuchung des einflusses der blutflussgeschwindigkeit auf die gefäßkühlung bei der radiofrequenzablation von lebertumoren," 2006.

[11] A. Loriaud, A. Denys, O. Seror, N. Vietti Violi, A. Digklia, R. Duran, H. Trillaud, and A. Hocquelet, "Hepatocellular carcinoma abutting large vessels: comparison of four percutaneous ablation systems," *International Journal of Hyperthermia*, vol. 34, no. 8, pp. 1171–1178, 2018.

[12] H.-W. Huang, "Influence of blood vessel on the thermal lesion formation during radiofrequency ablation for liver tumors," *Medical Physics*, vol. 40, no. 7, p. 073303, 2013.

[13] H. M. Luu, C. Klink, A. Moelker, W. Niessen, and T. Van Walsum, "Quantitative evaluation of noise reduction and vesselness filters for liver vessel segmentation

on abdominal cta images," *Physics in Medicine & Biology*, vol. 60, no. 10, p. 3905, 2015.
[14] Y.-H. Shao, K. Tsai, S. Kim, Y.-J. Wu, and K. Demissie, "Exposure to tomographic scans and cancer risks," *JNCI Cancer Spectrum*, vol. 4, no. 1, p. pkz072, 2020.
[15] M. H. Luu, T. van Walsum, H. S. Mai, D. Franklin, T. T. T. Nguyen, T. M. Le, A. Moelker, D. L. Vu, N. H. Le, Q. L. Tran, *et al.*, "Automatic scan range for dose-reduced multiphase ct imaging of the liver utilizing cnns and gaussian models," *Medical Image Analysis*, vol. 78, p. 102422, 2022.
[16] S. Survarachakan, E. Pelanis, Z. A. Khan, R. P. Kumar, B. Edwin, and F. Lindseth, "Effects of enhancement on deep learning based hepatic vessel segmentation," *Electronics*, vol. 10, no. 10, p. 1165, 2021.
[17] L. Quoc Anh, P. Xuan Loc, and L. Manh Ha, "Performance evaluation of deep learning algorithms for hepatic vessel segmentation in ct image," in *REV-ECIT*. REV, 2021, pp. 1–6.
[18] N. Sangsefidi, A. H. Foruzan, and A. Dolati, "Balancing the data term of graph-cuts algorithm to improve segmentation of hepatic vascular structures," *Computers in Biology and Medicine*, vol. 93, pp. 117–126, 2018.
[19] T. Kitrungrotsakul, X.-H. Han, Y. Iwamoto, L. Lin, A. H. Foruzan, W. Xiong, and Y.-W. Chen, "Vesselnet: A deep convolutional neural network with multi pathways for robust hepatic vessel segmentation," *Computerized Medical Imaging and Graphics*, vol. 75, pp. 74–83, 2019.
[20] J. Su, Z. Liu, J. Zhang, V. S. Sheng, Y. Song, Y. Zhu, and Y. Liu, "DV-Net: Accurate liver vessel segmentation via dense connection model with D-BCE loss function," *Knowledge-Based Systems*, p. 107471, 2021.
[21] W. Yu, B. Fang, Y. Liu, M. Gao, S. Zheng, and Y. Wang, "Liver vessels segmentation based on 3d residual U-NET," in *Proceedings of the IEEE International Conference on Image Processing (ICIP)*. IEEE, 2019, pp. 250–254.
[22] F. Isensee, P. F. Jaeger, S. A. Kohl, J. Petersen, and K. H. Maier-Hein, "nnU-Net: a self-configuring method for deep learning-based biomedical image segmentation," *Nature Methods*, vol. 18, no. 2, pp. 203–211, 2021.
[23] J. Wang, H. Lu, T. Li, and Z. Liang, "Sinogram noise reduction for low-dose CT by statistics-based nonlinear filters," in *Medical Imaging 2005: Image Processing*, vol. 5747. SPIE, 2005, pp. 2058–2066.
[24] J. Wang, T. Li, H. Lu, and Z. Liang, "Penalized weighted least-squares approach to sinogram noise reduction and image reconstruction for low-dose x-ray computed tomography," *IEEE Transactions on Medical Imaging*, vol. 25, no. 10, pp. 1272–1283, 2006.
[25] R. Manniesing, M. A. Viergever, and W. J. Niessen, "Vessel enhancing diffusion: A scale space representation of vessel structures," *Medical Image Analysis*, vol. 10, no. 6, pp. 815–825, 2006.
[26] H. Chen, Y. Zhang, M. K. Kalra, F. Lin, Y. Chen, P. Liao, J. Zhou, and G. Wang, "Low-dose CT with a residual encoder-decoder convolutional neural network," *IEEE Transactions on Medical Imaging*, vol. 36, no. 12, pp. 2524–2535, 2017.
[27] H. Shan, Y. Zhang, Q. Yang, U. Kruger, M. K. Kalra, L. Sun, W. Cong, and G. Wang, "3-D convolutional encoder-decoder network for low-dose CT via transfer learning from a 2-D trained network," *IEEE Transactions on Medical Imaging*, vol. 37, no. 6, pp. 1522–1534, 2018.
[28] N. Thanh-Trung, D.-H. Trinh, N. Linh-Trung, and M. Luong, "Low dose CT image denoising using deep convolutional neural networks with extended receptive fields," 2021.
[29] J. Leuschner, M. Schmidt, D. O. Baguer, and P. Maass, "Lodopab-ct, a benchmark dataset for low-dose computed tomography reconstruction," *Scientific Data*, vol. 8, no. 1, pp. 1–12, 2021.
[30] P. F. Christ, M. E. A. Elshaer, F. Ettlinger, S. Tatavarty, M. Bickel, P. Bilic, M. Rempfler, M. Armbruster, F. Hofmann, M. D'Anastasi, *et al.*, "Automatic liver and lesion segmentation in CT using cascaded fully convolutional neural networks and 3D conditional random fields," in *Proceedings of the International conference on medical image computing and computer-assisted intervention*. Springer, 2016, pp. 415–423.
[31] H. Shan, A. Padole, F. Homayounieh, U. Kruger, R. D. Khera, C. Nitiwarangkul, M. K. Kalra, and G. Wang, "Competitive performance of a modularized deep neural network compared to commercial algorithms for low-dose CT image reconstruction," *Nature Machine Intelligence*, vol. 1, no. 6, pp. 269–276, 2019.
[32] M. Antonelli, A. Reinke, S. Bakas, K. Farahani, B. A. Landman, G. Litjens, B. Menze, O. Ronneberger, R. M. Summers, B. van Ginneken, *et al.*, "The medical segmentation decathlon," *arXiv preprint arXiv:2106.05735*, 2021.
[33] A. Hamard, J. Frandon, A. Larbi, J. Goupil, H. De Forges, J.-P. Beregi, and J. Greffier, "Impact of ultra-low dose CT acquisition on semi-automated RECIST tool in the evaluation of malignant focal liver lesions," *Diagnostic and Interventional Imaging*, vol. 101, no. 7-8, pp. 473–479, 2020.
[34] G. Lavoué, "A local roughness measure for 3D meshes and its application to visual masking," *ACM Transactions on Applied Perception (TAP)*, vol. 5, no. 4, pp. 1–23, 2009.
[35] K. A. McGlynn, J. L. Petrick, and W. T. London, "Global epidemiology of hepatocellular carcinoma: an emphasis on demographic and regional variability," *Clinics in Liver Disease*, vol. 19, no. 2, pp. 223–238, 2015.

Le Quoc Anh is a Master's student at VNU University of Engineering and Technology (VNU-UET). He received his B.E. degree in Electronics and Communications Engineering from VNU-UET. Since 2020, he has been a member of the Advanced Institute of Engineering and Technology (AVITECH) of VNU-UET, where he works as a research assistant. His research interests include biomedical signal processing and medical image processing.

Pham Xuan Loc is currently a Master student at Vietnam National University-University of Engineering and Technology (VNU-UET). He received his B.E degree majoring in Computer Science and Engineering at the University of Aizu (UoA), Japan in 2019. Since 2020, he has been a member of the Faculty of Electronics and Telecommunications (FET, VNU-UET), where he is working as a research assistant and teaching assistant. His research interest is medical image analysis, with the main focus on the application of deep learning on liver computed tomography image analysis for liver cancer treatment support.

Luu Manh Ha was born in Hanoi, Vietnam. He completed his Bachelor program in Faculty of Electronics and telecommunications at VNU University of Engineering and Technology (VNU-UET) in 2007. He continued the work as a researcher and received his MSc degree in Electronic Engineering from VNU-UET in 2010. He finished his Ph.D. in the BIGR group, Erasmus Medical Center, Rotterdam, the Netherlands in 2017. He has been working for VNU-UET in Vietnam since 2017 as a lecturer and a researcher. Since 2020, he has been working as a postdoc in AVITECH institute (UET-VNU). His research scheme is applications of AI and digital signal processing techniques in biomedical image analysis, mainly focuses on abdominal images (CT, US, SPECT) of the liver, biosignal processing, retinal image processing and chromosome image processing.